

Floquet engineering of a dynamical Z_2 lattice gauge field with ultracold atoms

Xiangxiang Sun(孙祥祥), Hao-Yue Qi(齐浩月), Pengfei Zhang(张鹏飞), and Wei Zheng(郑炜)

Citation: Chin. Phys. B, 2024, 33 (**11**): 110304. DOI: 10.1088/1674-1056/ad7576
Journal homepage: http://cpb.iphy.ac.cn; http://iopscience.iop.org/cpb

What follows is a list of articles you may be interested in

Variational data encoding and correlations in quantum-enhanced machine learning

Ming-Hao Wang(王明浩) and Hua Lü(吕桦)
Chin. Phys. B, 2024, 33 (**9**): 090307. DOI: 10.1088/1674-1056/ad5c3b

Preparation of entangled W states based on the cavity QED system

Ke Li(李可) and Jun-Long Zhao(赵军龙)
Chin. Phys. B, 2024, 33 (**9**): 090306. DOI: 10.1088/1674-1056/ad50bf

Quantum computation and simulation with vibrational modes of trapped ions

Wentao Chen(陈文涛), Jaren Gan, Jing-Ning Zhang(张静宁), Dzmitry Matuskevich, and Kihwan Kim(金奇奂)
Chin. Phys. B, 2021, 30 (**6**): 060311. DOI: 10.1088/1674-1056/ac01e3

Review of quantum simulation based on Rydberg many-body system

Zheng-Yuan Zhang(张正源), Dong-Sheng Ding(丁冬生), and Bao-Sen Shi(史保森)
Chin. Phys. B, 2021, 30 (**2**): 020307. DOI: 10.1088/1674-1056/abd744

Nuclear magnetic resonance for quantum computing: Techniques and recent achievements

Tao Xin(辛涛), Bi-Xue Wang(王碧雪), Ke-Ren Li(李可仁), Xiang-Yu Kong(孔祥宇), Shi-Jie Wei(魏世杰), Tao Wang(王涛), Dong Ruan(阮东), Gui-Lu Long(龙桂鲁)
Chin. Phys. B, 2018, 27 (**2**): 020308. DOI: 10.1088/1674-1056/27/2/020308

Floquet engineering of a dynamical Z_2 lattice gauge field with ultracold atoms

Xiangxiang Sun(孙祥祥)[1,2], Hao-Yue Qi(齐浩月)[1,2], Pengfei Zhang(张鹏飞)[3,4,5,†], and Wei Zheng(郑炜)[1,2,5,‡]

[1] *Hefei National Laboratory for Physical Sciences at the Microscale and Department of Modern Physics, University of Science and Technology of China, Hefei* 230026, *China*
[2] *CAS Center for Excellence in Quantum Information and Quantum Physics, University of Science and Technology of China, Hefei* 230026, *China*
[3] *Department of Physics, Fudan University, Shanghai* 200438, *China*
[4] *Shanghai Qi Zhi Institute, AI Tower, Xuhui District, Shanghai* 200232, *China*
[5] *Hefei National Laboratory, Hefei 230088, China*

(Received 24 May 2024; revised manuscript received 8 August 2024; accepted manuscript online 30 August 2024)

Gauge field theory is a fundamental concept in modern physics, attracting many theoretical and experimental efforts towards its simulation. In this paper we propose that a simple model, in which fermions coupled to a dynamical lattice gauge field, can be engineered via the Floquet approach. The model possesses both an independent Maxwell term and local Z_2 gauge symmetry. Our proposal relies on a species-dependent optical lattice, and can be achieved in one, two or three dimensions. By a unitary transformation, this model can be mapped into a non-interacting composite fermion system with fluctuating background charge. With the help of this composite fermion picture, two characteristic observations are predicted. One is radio-frequency spectroscopy, which exhibits no dispersion in all parameter regimes. The second is dynamical localization, which depends on the structure of the initial states.

Keywords: gauge theory, quantum simulations

PACS: 03.67.Ac, 11.15.Ha **DOI:** 10.1088/1674-1056/ad7576

1. Introduction

Gauge field theory is one of the most important cornerstones of modern physics. On one hand, gauge theory has successfully described the fundamental interactions within the standard model of high-energy physics. On the other hand, lattice gauge theory can also emerge from the low-energy physics of strongly correlated systems.[1] For example, $U(1)$ lattice gauge theory can effectively describe the collective fluctuations of frustrated magnetism,[2–4] quantum spin liquids,[5–8] and the quantum dimer model.[9,10] In fact, dynamical gauge fields enter the theory naturally in so-called slave-particle decomposition, whereby the original particles are fractionalized into slave degrees of freedom. The relative phase between the slave particles introduces local gauge invariance. Understanding the real-time dynamics of lattice gauge fields is a notable challenge due to the limits of classical computational methods. This has stimulated efforts on quantum simulation of gauge fields in various engineered systems.[11–15]

In cold atom systems, static artificial gauge fields have been simulated in recent years, including electrical field,[16] magnetic field[17] and even spin–orbit couplings.[18,19] However the configurations of those gauge fields are fixed by the external laser or system geometry. Therefore these fields have no dynamics, and cannot mediate the interaction between atoms. The Chicago and ETH groups have realized density-dependent gauge fields by periodic modulation of the optical lattice or the interaction,[20,21] while the Stanford group has realized a cavity-induced one-dimensional spin–orbit-coupled Bose–Einstein condensate.[22] In these experiments, the artificial gauge fields are no longer static but can fluctuate with time. However, local gauge invariance, the key ingredient of gauge theory, is still missing in those simulations. Recently several groups have successfully simulated a dynamical lattice gauge field with local Z_2[23] and $U(1)$[24,25] gauge symmetry in optical lattices, and unusual thermalization and confinement dynamics in $U(1)$ lattice gauge theories have been observed.[26–28] However, the realized Z_2 lattice gauge theory[23] is restricted to a double-well geometry. Thus it is still challenging to simulate the dynamical Z_2 gauge field in a scalable way or in higher dimensions.

In this paper, we propose that a simple model, in which fermions interact with a dynamical lattice gauge field with local Z_2 symmetry, can be engineered via the Floquet approach. Unlike a previous experiment in a double well,[23] our setup is scalable and can be applied in one, two or three dimensions. By a unitary transformation, this model can be mapped into a non-interacting composite fermion system with fluctuating background charge. With the help of this composite fermion picture, two characteristic observations are predicted. One is that the radio-frequency spectrum of the fermions exhibits no dispersion in all parameter regimes, reflecting the local symmetry of the model. The other is the dynamical localization

†Corresponding author. E-mail: PengfeiZhang.physics@gmail.com
‡Corresponding author. E-mail: zw8796@ustc.edu.cn

© 2024 Chinese Physical Society and IOP Publishing Ltd

of the fermions, which depends on the structure of the initial states.

This paper is organized as follows. We propose a feasible model and demonstrate its capability to simulate Z_2 lattice gauge theory in Section 2. Then we further discuss the symmetry of our model and map this model into a non-interacting composite fermion system with fluctuating background charge in Section 3. Next, in Section 4, we calculate the radio-frequency spectroscopy, revealing no dispersion. Dynamical localization is predicted in Section 5. Finally our results are summarized in Section 6.

2. Experimental setup

In this section, we introduce our model designed for realizing the Z_2 lattice gauge field. Our scheme consists of two kinds of atoms. One is mobile spinless fermions denoted as $\hat{c}_{\boldsymbol{r}}$, used to simulate the matter field; the other is localized spin-1/2 fermions denoted as $\hat{d}_{\boldsymbol{r},\uparrow(\downarrow)}$, to simulate the gauge field. The fermions are trapped in a species-dependent cubic optical lattice.

By carefully tuning the optical lattice, one can greatly suppress the hopping of the $\hat{d}$-fermions while retaining the hopping of the $\hat{c}$-fermions. A radio-frequency field is applied to couple spin-up and spin-down states of the $\hat{d}$-fermions. The resulting Hamiltonian, after the tight-binding approximation, reads $\hat{H}(t)=\hat{H}_0+\hat{H}_{\rm I}+\hat{V}(t)$:

$$H_0 = J\sum_{\boldsymbol{r},i}\hat{c}^{\dagger}_{\boldsymbol{r}+\boldsymbol{a}_i}\hat{c}_{\boldsymbol{r}}+\Omega\sum_{\boldsymbol{r}}\hat{d}^{\dagger}_{\boldsymbol{r},\uparrow}\hat{d}_{\boldsymbol{r},\downarrow}+\text{h.c.}, \tag{1}$$

$$\hat{H}_{\rm I} = \sum_{\boldsymbol{r}}\left(U_{\uparrow}\hat{n}^{d}_{\boldsymbol{r},\uparrow}\hat{n}^{c}_{\boldsymbol{r}}+U_{\downarrow}\hat{n}^{d}_{\boldsymbol{r},\downarrow}\hat{n}^{c}_{\boldsymbol{r}}\right), \tag{2}$$

$$\hat{V}(t) = \sum_{\boldsymbol{r}}\left[\boldsymbol{F}(t)\cdot\boldsymbol{r}\hat{n}^{c}_{\boldsymbol{r}}+h(t)\left(\hat{n}^{d}_{\boldsymbol{r},\uparrow}-\hat{n}^{d}_{\boldsymbol{r},\downarrow}\right)\right], \tag{3}$$

where $\boldsymbol{a}_i=a\boldsymbol{e}_i$ is the basic vector of the cubic lattice and $U_{\uparrow(\downarrow)}$ is the on-site interaction between the $\hat{c}$-fermions and spin-up (-down) $\hat{d}$-fermions. We prepare the initial state such that the particle number of the $\hat{d}$-fermion at each site is constrained to be unity, $\hat{n}^{d}_{\boldsymbol{r},\uparrow}+\hat{n}^{d}_{\boldsymbol{r},\downarrow}=1$. Since the hopping of $\hat{d}$-fermions is suppressed, during the evolution the occupation of $\hat{d}$-fermions at each site is conserved to be one. As a result the interaction between spin-up and spin-down $\hat{d}$-fermions is irrelevant in this study.

There are two periodic driving terms. One is an oscillating Zeeman field, $h(t)=h\cos(\omega t)$, which is applied on the $\hat{d}$-fermions. Another is a periodic driving force, $\boldsymbol{F}(t)=F\sin(\omega t)\sum_{i=1}^{3}\boldsymbol{e}_i$, which can be realized by linearly polarized shaking of the optical lattice. The two driving terms share the same frequency, with a relative phase shift ϕ. Specifically, the driving frequency is chosen to be two-photon resonant with the interaction difference $2\omega=U_{\uparrow}-U_{\downarrow}$ (here we set $\hbar=1$).

To deal with this time periodic driven quantum system, we first make a rotating wave transformation

$$\hat{R}(t)=\exp\left\{-\mathrm{i}\int_0^t \mathrm{d}\tau[\hat{H}_{\rm I}+\hat{V}(\tau)]\right\} \tag{4}$$

to eliminate the interaction and driving terms. We obtain the Hamiltonian in the rotating frame as

$$\begin{aligned}\hat{H}_{\rm rw}(t) &= \hat{R}(t)\left[\hat{H}(t)-\mathrm{i}\partial_t\right]\hat{R}^{\dagger}(t)\\ &= J\sum_{\boldsymbol{r},i}\hat{c}^{\dagger}_{\boldsymbol{r}+\boldsymbol{a}_i}\hat{P}^{d}_{\boldsymbol{r}+\boldsymbol{a}_i}\hat{P}^{d}_{\boldsymbol{r}}\hat{c}_{\boldsymbol{r}}\,\mathrm{e}^{\mathrm{i}\frac{Fa}{\hbar\omega}\sin(\omega t)}\\ &\quad+\Omega\sum_{\boldsymbol{r}}\hat{d}^{\dagger}_{\boldsymbol{r},\uparrow}\hat{P}^{c}_{\boldsymbol{r},\uparrow}\hat{P}^{c}_{\boldsymbol{r},\uparrow}\hat{d}_{\boldsymbol{r},\downarrow}\,\mathrm{e}^{\mathrm{i}\frac{2h}{\omega}\cos(\omega t)}+\text{h.c.},\end{aligned} \tag{5}$$

where $\hat{P}^{d}_{\boldsymbol{r}}=\hat{n}^{d}_{\boldsymbol{r},\uparrow}\mathrm{e}^{-\mathrm{i}U_{\uparrow}t}+\hat{n}^{d}_{\boldsymbol{r},\downarrow}\mathrm{e}^{-\mathrm{i}U_{\downarrow}t}$, and $\hat{P}^{c}_{\boldsymbol{r},\uparrow(\downarrow)}=(1-\hat{n}^{c}_{\boldsymbol{r}})+\hat{n}^{c}_{\boldsymbol{r}}\mathrm{e}^{-\mathrm{i}U_{\uparrow(\downarrow)}t}$ are oscillating phase factors, depending on the occupation of $\hat{d}$-fermions and $\hat{c}$-fermions, respectively.

Subsequently, we apply the high-frequency expansion to derive the time-independent effective Hamiltonian as $\hat{H}_{\rm eff}=\hat{H}^{(0)}_{\rm rw}+\sum_{m=1}^{\infty}\left[\hat{H}^{(m)}_{\rm rw},\hat{H}^{(-m)}_{\rm rw}\right]/(m\omega)+\cdots$, where $\hat{H}^{(m)}_{\rm rw}=\frac{1}{T}\int_0^T \mathrm{d}t\hat{H}_{\rm rw}(t)\,\mathrm{e}^{-\mathrm{i}m\omega t}$ is the Fourier component of the Hamiltonian. Here we consider the high-frequency limit, such that one can only keep to zeroth order, obtaining

$$\begin{aligned}\hat{H}_{\rm eff} &\approx \hat{H}^{(0)}_{\rm rw}\\ &= J\sum_{\boldsymbol{r},i}\{\mathcal{J}_0(\lambda_F)(\hat{n}^{d}_{\boldsymbol{r}+\boldsymbol{a}_i,\uparrow}\hat{n}^{d}_{\boldsymbol{r},\uparrow}+\hat{n}^{d}_{\boldsymbol{r}+\boldsymbol{a}_i,\downarrow}\hat{n}^{d}_{\boldsymbol{r},\downarrow})\\ &\quad-\mathcal{J}_2(\lambda_F)(\hat{n}^{d}_{\boldsymbol{r}+\boldsymbol{a}_i,\downarrow}\hat{n}^{d}_{\boldsymbol{r},\uparrow}+\hat{n}^{d}_{\boldsymbol{r}+\boldsymbol{a}_i,\uparrow}\hat{n}^{d}_{\boldsymbol{r},\downarrow})\}\hat{c}^{\dagger}_{\boldsymbol{r}+\boldsymbol{a}_i}\hat{c}_{\boldsymbol{r}}\\ &\quad+\Omega\sum_{\boldsymbol{r}}\{\mathcal{J}_0(\lambda_h)(1-\hat{n}^{c}_{\boldsymbol{r}})+\mathcal{J}_2(\lambda_h)\hat{n}^{c}_{\boldsymbol{r}}\}\hat{d}^{\dagger}_{\boldsymbol{r},\uparrow}\hat{d}_{\boldsymbol{r},\downarrow}\\ &\quad+\text{h.c.},\end{aligned} \tag{6}$$

where $\lambda_F=Fa/\omega$, $\lambda_h=2h/\omega$ and $\mathcal{J}_m(\lambda)$ is the Bessel function.

The corresponding physical processes are illustrated in Fig. 1. The lattice shaking largely modifies the hopping of the $\hat{c}$-fermions so that it is dependent on the spin configuration of the localized $\hat{d}$-fermions. If the spins polarize in the same direction on the nearest-neighbor sites, there is no energy offset for the $\hat{c}$-fermions. Consequently, the lattice shaking merely renormalizes the bare hopping to $J\mathcal{J}_0(\lambda_F)$ (see Figs. 1(a) and 1(b)). Conversely, if the spin polarizations are opposite to each other, energy imbalance of $\pm\left(U_{\uparrow}-U_{\downarrow}\right)$ arises. Then the $\hat{c}$-fermions will absorb (emit) two energy quanta from (to) shaking to hoppig, resulting in an amplitude of $J\mathcal{J}_2(\lambda_F)$. Moreover, the phase of these two energy quanta is imprinted to the hopping (see Figs. 1(c) and 1(d)).

Similar to the hopping process, the spin flip of the $\hat{d}$-fermions is also modified by the oscillating Zeeman field. The modification is dependent on the charge density of the $\hat{c}$-fermions. If $n^{c}_{\boldsymbol{r}}=0$, the Rabi frequency is merely renormalized by the oscillating Zeeman field (see Fig. 1(e)). If $n^{c}_{\boldsymbol{r}}=1$, two energy quanta are absorbed(emitted) to assist the local spin flip (see Fig. 1(f)).

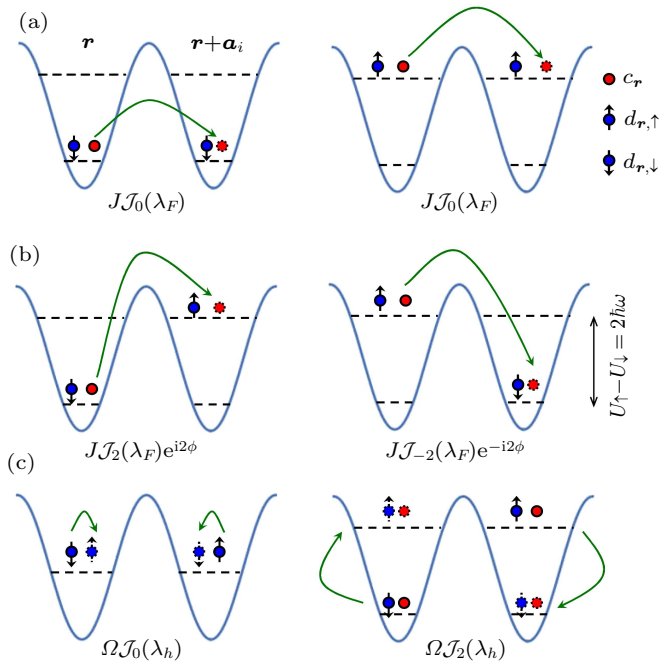


Fig. 1. The physical processes for the effective Hamiltonian. Red circles represent the spinless $\hat{c}$-fermions hopping in the lattice, while blue circles with an arrow represent the spinful localized $\hat{d}$-fermions. (a), (b) The renormalized hopping of $\hat{c}$-fermions in the case of same-spin polarization of $\hat{d}$-fermions between the neighboring sites. (c), (d) Shaking assistant hopping of $\hat{c}$-fermions in the case of opposite spin polarization of $\hat{d}$-fermions. (e) The renormalized spin flip of $\hat{d}$-fermions in the absence of $\hat{c}$-fermions. (f) The shaking assistant spin flip of $\hat{d}$-fermions in the presence of $\hat{c}$-fermions.

Then we fine tune the parameter as $\mathcal{J}_0(\lambda_F) = \mathcal{J}_2(\lambda_F)$ and $\mathcal{J}_0(\lambda_h) = \mathcal{J}_2(\lambda_h)$. This can be achieved by choosing $\lambda_F = \lambda_h = 1.84118$ or 5.33144 (see Fig. 2). As a result, we obtain

$$\begin{aligned}\hat{H}_{\text{eff}} &= J\mathcal{J}_2(\lambda_F)\sum_{\boldsymbol{r},i}\left[\hat{n}^d_{\boldsymbol{r}+\boldsymbol{a}_i,\uparrow} - \left(1-\hat{n}^d_{\boldsymbol{r}+\boldsymbol{a}_i,\uparrow}\right)\right] \\ &\times \left[\hat{n}^d_{\boldsymbol{r},\uparrow} - \left(1-\hat{n}^d_{\boldsymbol{r},\uparrow}\right)\right]\hat{c}^\dagger_{\boldsymbol{r}+\boldsymbol{a}_i}\hat{c}_{\boldsymbol{r}} \\ &+ \Omega\mathcal{J}_2(\lambda_h)\sum_{\boldsymbol{r}}\hat{d}^\dagger_{\boldsymbol{r},\uparrow}\hat{d}_{\boldsymbol{r},\downarrow} + \text{h.c.} \end{aligned} \tag{7}$$

Note that the total number of the $\hat{d}$-fermions at each site is fixed $\hat{n}^d_{\boldsymbol{r},\uparrow} + \hat{n}^d_{\boldsymbol{r},\downarrow} = 1$, thus the effective Hamiltonian can be further simplified as

$$\begin{aligned}\hat{H}_{\text{eff}} &= J\mathcal{J}_2(\lambda_F)\sum_{\boldsymbol{r},j}\left(\hat{n}^d_{\boldsymbol{r}+\boldsymbol{a}_i,\uparrow} - \hat{n}^d_{\boldsymbol{r}+\boldsymbol{a}_i,\downarrow}\right) \\ &\times \left(\hat{n}^d_{\boldsymbol{r},\uparrow} - \hat{n}^d_{\boldsymbol{r},\downarrow}\right)\hat{c}^\dagger_{\boldsymbol{r}+\boldsymbol{a}_i}\hat{c}_{\boldsymbol{r}} \\ &+ \Omega\mathcal{J}_2(\lambda_h)\sum_{\boldsymbol{r}}\hat{d}^\dagger_{\boldsymbol{r},\uparrow}\hat{d}_{\boldsymbol{r},\downarrow} + \text{h.c.} \end{aligned} \tag{8}$$

Then we use the Pauli matrix to represent the spin degree of freedom of the local $\hat{d}$-fermions as $\sigma^z_{\boldsymbol{r}} = \hat{n}^d_{\boldsymbol{r},\uparrow} - \hat{n}^d_{\boldsymbol{r},\downarrow}$, $\sigma^x_{\boldsymbol{r}} = \hat{d}^\dagger_{\boldsymbol{r},\uparrow}\hat{d}_{\boldsymbol{r},\downarrow} + \hat{d}^\dagger_{\boldsymbol{r},\downarrow}\hat{d}_{\boldsymbol{r},\uparrow}$, and $\sigma^y_{\boldsymbol{r}} = -\text{i}(\hat{d}^\dagger_{\boldsymbol{r},\uparrow}\hat{d}_{\boldsymbol{r},\downarrow} - \hat{d}^\dagger_{\boldsymbol{r},\downarrow}\hat{d}_{\boldsymbol{r},\uparrow})$. So the effective Hamiltonian can be expressed as

$$\hat{H}_{\text{eff}} = \tilde{J}\sum_{\boldsymbol{r},i}\sigma^z_{\boldsymbol{r}+\boldsymbol{a}_i}\sigma^z_{\boldsymbol{r}}(\hat{c}^\dagger_{\boldsymbol{r}+\boldsymbol{a}_i}\hat{c}_{\boldsymbol{r}} + \text{h.c.}) + \tilde{\Omega}\sum_{\boldsymbol{r}}\sigma^x_{\boldsymbol{r}}, \tag{9}$$

where $\tilde{J} = J\mathcal{J}_0(\lambda_F)$ and $\tilde{\Omega} = \Omega\mathcal{J}_0(\lambda_h)$. This Hamiltonian describes a dynamic Z_2 lattice gauge field coupled to spinless fermions. We note that the fermion hopping phase factor $e^{i\theta} \sim \sigma^z_{\boldsymbol{r}+\boldsymbol{a}_i}\sigma^z_{\boldsymbol{r}}$ could be ± 1. That means the Peierls phase θ is either 0 or π, rather than a continuous value in $U(1)$ gauge theory. Moreover, $\sigma^z_{\boldsymbol{r}+\boldsymbol{a}_i}\sigma^z_{\boldsymbol{r}}$ does not commute with the Maxwell term, $\tilde{\Omega}\sum_{\boldsymbol{r}}\sigma^x_{\boldsymbol{r}}$, in the Hamiltonian. As a result, unlike the static gauge field, the Peierls phase in this lattice will fluctuate in real-time dynamics.

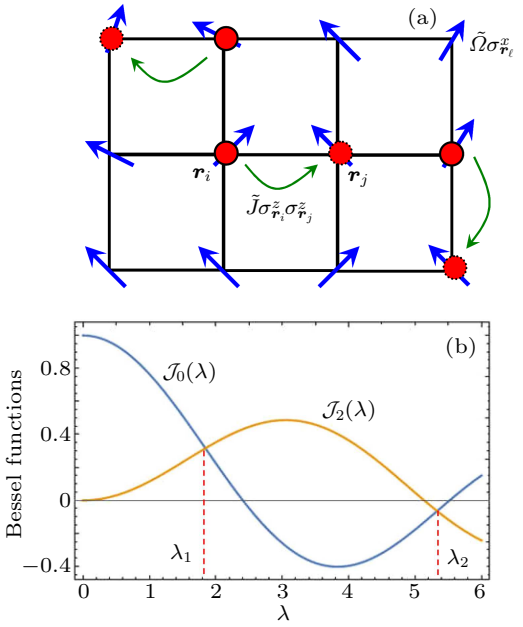


Fig. 2. (a) Illustration of the Z_2 lattice gauge theory given by Hamiltonian (9). Local spins live on each lattice site. Spinless $\hat{c}$-fermions can hop between the lattice sites. The hopping amplitude depends on the configuration of the local spins. (b) Fine tuning of modulations. The solutions of $\mathcal{J}_0(\lambda) = \mathcal{J}_2(\lambda)$ are $\lambda_1 = 1.84118$ and $\lambda_2 = 5.33144$.

The Hamiltonian (9) can also be dualed to the standard Z_2 lattice gauge theory, where gauge fields τ are defined on the link, with coupling terms $\hat{c}^\dagger_{\boldsymbol{r}+\boldsymbol{a}_i}\hat{c}_{\boldsymbol{r}}\tau^z_{\boldsymbol{r}}$, star terms $\prod_+ \tau^x_{\boldsymbol{r}+\boldsymbol{a}_i/2}$ and flux terms $\prod_\square \tau^z_{\boldsymbol{r}}$ in the Hamiltonian. We could define the duality $\tau^z_{\boldsymbol{r}+\boldsymbol{a}_i/2} = \sigma^z_{\boldsymbol{r}+\boldsymbol{a}_i}\sigma^z_{\boldsymbol{r}}$. The first term in Hamiltonian (9) becomes the standard coupling term and the second term becomes the star term. Moreover, the definition imposes the constraint that $\prod_\square \tau^z_{\boldsymbol{r}} = 1$, which is equivalent to having a large flux term.

3. Symmetry

As we have emphasized, in contrast to density-dependent gauge fields that lack local gauge symmetry,[20–22] our model exhibits a local Z_2 gauge symmetry at each site. The gauge transformation operator is given by

$$\hat{G}_{\boldsymbol{r}} = e^{i\pi\hat{n}^c_{\boldsymbol{r}}}\sigma^x_{\boldsymbol{r}}. \tag{10}$$

Under this gauge transformation, the operators transform as

$$\hat{G}_{\boldsymbol{r}}\hat{c}_{\boldsymbol{r}}\hat{G}^\dagger_{\boldsymbol{r}} = -\hat{c}_{\boldsymbol{r}}, \tag{11}$$

$$\hat{G}_{\boldsymbol{r}}\sigma^x_{\boldsymbol{r}}\hat{G}^\dagger_{\boldsymbol{r}} = \sigma^x_{\boldsymbol{r}}, \tag{12}$$

$$\hat{G}_{\boldsymbol{r}}\sigma^z_{\boldsymbol{r}}\hat{G}^\dagger_{\boldsymbol{r}} = -\sigma^z_{\boldsymbol{r}}. \tag{13}$$

With the transform formula given above, it is straightforward to verify that

$$[\hat{G}_{\boldsymbol{r}}, \hat{H}_{\text{eff}}] = 0, \tag{14}$$

$$[\hat{G}_{\boldsymbol{r}_2}, \hat{G}_{\boldsymbol{r}_1}] = 0 \tag{15}$$

for any given site. That means the the Hamiltonian and $\hat{G}_{\boldsymbol{r}}$ can share the same set of eigenstates

$$\hat{H}_{\text{eff}} |\psi_m(\boldsymbol{g})\rangle = E_m(\boldsymbol{g}) |\psi_m(\boldsymbol{g})\rangle, \tag{16}$$

$$\hat{G}_{\boldsymbol{r}} |\psi_m(\boldsymbol{g})\rangle = g_{\boldsymbol{r}} |\psi_m(\boldsymbol{g})\rangle, \tag{17}$$

where vector $\boldsymbol{g} = (g_{\boldsymbol{r}_1}, g_{\boldsymbol{r}_2}, \ldots)$ labels one gauge sector with gauge charge $g_{\boldsymbol{r}} = \pm 1$. This separates the Hilbert space, spanned by the eigenstates of the effective Hamiltonian, into distinct gauge sectors. In each sector, $\hat{G}_{\boldsymbol{r}}$ is a good quantum number, and thus can be replaced by its eigenvalues $g_{\boldsymbol{r}}$. As a result, in this gauge sector, Eq. (10) can be expressed as

$$g_{\boldsymbol{r}} = \mathrm{e}^{\mathrm{i}\pi\hat{n}^c_{\boldsymbol{r}}} \sigma^x_{\boldsymbol{r}}. \tag{18}$$

This is nothing but the Z_2 Gauss law similar to electrodynamics. Here $\mathrm{e}^{\mathrm{i}\pi\hat{n}^c_{\boldsymbol{r}}}$ is the Z_2 charge carried by the matter field, $g_{\boldsymbol{r}}$ is the local gauge charge and $\sigma^x_{\boldsymbol{r}}$ is the electrical field. In real-world scenarios, we are constrained in the gauge-invariant subsector, where the background charge is zero. However, in our synthetic world we can prepare the initial states at different subspaces, or even the superposition of several subsectors. That leads to richer dynamics of the gauge field.

Making a global unitary transformation,[33] $\hat{U} = \exp(\mathrm{i}\frac{\pi}{2}\sum_{\boldsymbol{r}} \sigma^z_{\boldsymbol{r}} \hat{n}^c_{\boldsymbol{r}})$, we find that the matter field and the gauge field are bound

$$\hat{U}\hat{c}_{\boldsymbol{r}}\hat{U}^\dagger = -\mathrm{i}\sigma^z_{\boldsymbol{r}}\hat{c}_{\boldsymbol{r}}, \tag{19}$$

$$\hat{U}\sigma^z_{\boldsymbol{r}}\hat{U}^\dagger = \sigma^z_{\boldsymbol{r}}, \tag{20}$$

$$\hat{U}\sigma^x_{\boldsymbol{r}}\hat{U}^\dagger = \sigma^x_{\boldsymbol{r}}(1 - 2\hat{n}_{\boldsymbol{r}}). \tag{21}$$

As a result, the Hamiltonian and $\hat{G}_{\boldsymbol{r}}$ are transformed into

$$\begin{aligned}\hat{H}' &= \hat{U}\hat{H}_{\text{eff}}\hat{U}^\dagger = \tilde{J}\sum_{\boldsymbol{r},i}(\hat{c}^\dagger_{\boldsymbol{r}+\boldsymbol{a}_i}\hat{c}_{\boldsymbol{r}} + \text{h.c.}) \\ &\quad + \tilde{\Omega}\sum_{\boldsymbol{r}} \sigma^x_{\boldsymbol{r}}(1 - 2\hat{n}_{\boldsymbol{r}}),\end{aligned} \tag{22}$$

$$\hat{G}'_{\boldsymbol{r}} = \hat{U}\hat{G}_{\boldsymbol{r}}\hat{U}^\dagger = \sigma^x_{\boldsymbol{r}}. \tag{23}$$

Note that, after transformation, the Hamiltonian explicitly includes local gauge transformation operator $\hat{G}'_{\boldsymbol{r}}$, which is now $\sigma^x_{\boldsymbol{r}}$. Thus in one particular gauge sector we replace $\sigma^x_{\boldsymbol{r}}$ by its eigenvalues $g_{\boldsymbol{r}}$, obtaining

$$\hat{H}_{\text{sub}}(\boldsymbol{g}) = \tilde{J}\sum_{\boldsymbol{r},i}(\hat{c}^\dagger_{\boldsymbol{r}+\boldsymbol{a}_i}\hat{c}_{\boldsymbol{r}} + \text{h.c.}) - 2\tilde{\Omega}\sum_{\boldsymbol{r}} g_{\boldsymbol{r}}\hat{n}^c_{\boldsymbol{r}}, \tag{24}$$

where a constant term $\tilde{\Omega}\sum_{\boldsymbol{r}} g_{\boldsymbol{r}}$ has been ignored.

By being constrained in one gauge sector, this lattice gauge model is mapped into non-interacting fermions moving in the potential of the background gauge charges. These fermions are so-called 'orthogonal' fermions,[29–32] which are a composite of local spins and $\hat{c}$-fermions. This mapping is similar to the integral out of the longitudinal electrical field to obtain the Coulomb interaction in Maxwell's theory. In our model, there is no Coulomb interaction between the particles, but only coupling between the matter field and the background charges. Thus the eigenstates of the system can be expressed as

$$|\psi_m(\boldsymbol{g})\rangle = \hat{U}^\dagger |\varphi_m(\boldsymbol{g})\rangle \otimes |\boldsymbol{g}\rangle, \tag{25}$$

where $|\varphi_m(\boldsymbol{g})\rangle$ is the eigenstate of orthogonal fermions in the gauge sector labeled by $\boldsymbol{g}$, $\hat{H}_{\text{sub}}(\boldsymbol{g})|\varphi_m(\boldsymbol{g})\rangle = E_m(\boldsymbol{g})|\varphi_m(\boldsymbol{g})\rangle$. And $|\boldsymbol{g}\rangle$ is the spin state, $|\boldsymbol{g}\rangle = \prod_{\boldsymbol{r}}(|\uparrow\rangle_{\boldsymbol{r}} + g_{\boldsymbol{r}}|\downarrow\rangle_{\boldsymbol{r}})/\sqrt{2}$, satisfying $\hat{G}'_{\boldsymbol{r}} = \sigma^x_{\boldsymbol{r}}|\boldsymbol{g}\rangle = g_{\boldsymbol{r}}|\boldsymbol{g}\rangle$.

At the half-filling, we numerically find the ground state as

$$|\psi_{\text{gs}}\rangle = \hat{U}^\dagger |\text{CDW}\rangle \otimes |\text{SDW}\rangle \tag{26}$$

in a one-dimensional lattice. The local spins form a spin density wave (SDW)

$$|\text{SDW}\rangle = \prod_{\boldsymbol{r}} \frac{|\uparrow\rangle_{\boldsymbol{r}} + \mathrm{e}^{\mathrm{i}\boldsymbol{Q}\cdot\boldsymbol{r}}|\downarrow\rangle_{\boldsymbol{r}}}{\sqrt{2}}, \tag{27}$$

where $\boldsymbol{Q} = \sum_{i=1}^d \frac{\pi}{a}\boldsymbol{e}_i$. This gives staggered background gauge charges, $\hat{G}'_{\boldsymbol{r}}|\text{SDW}\rangle = \mathrm{e}^{\mathrm{i}\boldsymbol{Q}\cdot\boldsymbol{r}}|\text{SDW}\rangle$. The orthogonal fermions form a charge density wave (CDW)

$$|\text{CDW}\rangle = \prod_{\boldsymbol{k}} \hat{\alpha}^\dagger_{\text{low}}(\boldsymbol{k})|0\rangle. \tag{28}$$

Here

$$\hat{\alpha}^\dagger_{\text{low},\boldsymbol{k}} = \cos\frac{\theta_{\boldsymbol{k}}}{2}\hat{c}^\dagger_{\boldsymbol{k}} - \sin\frac{\theta_{\boldsymbol{k}}}{2}\hat{c}^\dagger_{\boldsymbol{k}+\boldsymbol{Q}},$$

with

$$\tan\theta_{\boldsymbol{k}} = -\frac{\tilde{J}}{\tilde{\Omega}}\sum_{i=1}^d \cos(k_i a).$$

This ground state can be generalized to two and three dimensions. It can be understood in two limits. First if $\tilde{J} \to 0$, the ground states have $\langle\hat{n}_{\boldsymbol{r}}\rangle = 1\ (0)$, as $g_{\boldsymbol{r}} = +1\ (-1)$ to lower the on-site energy. There are innumerable states possessing the same energy, but for a finite $\tilde{J}$ the SDW configuration will minimize the kinetic energy at the half-filling. Second, at $\tilde{\Omega} \to 0$, the ground state is a Fermi sea of orthogonal fermions. When opening $\tilde{\Omega}$, the SDW will scatter the orthogonal fermions by a momentum $\boldsymbol{Q}$. At the half-filling, this matches the Fermi surface nesting, leading to gap opening and a CDW.

4. Radio-frequency spectroscopy

The effective Hamiltonian introduced above has two intriguing properties, one of which is absence of a dispersion relationship.[34] This property will be the focus of this section. To initiate our discussion, let us recall the spectral function given by

$$A_{\text{ab}}(\boldsymbol{k},\omega) = +\mathrm{i}\int \mathrm{d}t \sum_{\boldsymbol{r}} G^>(\boldsymbol{r},t)\,\mathrm{e}^{-\mathrm{i}(\boldsymbol{k}\cdot\boldsymbol{r}-\omega t)}, \tag{29}$$

$$A_{\text{em}}(\boldsymbol{k},\omega) = -\mathrm{i}\int \mathrm{d}t \sum_{\boldsymbol{r}} G^<(\boldsymbol{r},t)\,\mathrm{e}^{-\mathrm{i}(\boldsymbol{k}\cdot\boldsymbol{r}-\omega t)}. \tag{30}$$

Here the Green functions $G^>(\boldsymbol{r},t)$ and $G^<(\boldsymbol{r},t)$ are given by

$$\mathrm{i}G^{>}(\boldsymbol{r}_2-\boldsymbol{r}_1,t) = +\left\langle \hat{c}_{\boldsymbol{r}_2}(t)\hat{c}^{\dagger}_{\boldsymbol{r}_1}(0)\right\rangle_{\beta} = +\frac{1}{Z}\sum_{\boldsymbol{g},m} \mathrm{e}^{-\beta E_m(\boldsymbol{g})}\langle\psi_m(\boldsymbol{g})|\,\mathrm{e}^{\mathrm{i}\hat{H}_{\mathrm{eff}}t}\hat{c}_{\boldsymbol{r}_2}\mathrm{e}^{-\mathrm{i}\hat{H}_{\mathrm{eff}}t}\hat{c}^{\dagger}_{\boldsymbol{r}_1}|\psi_m(\boldsymbol{g})\rangle\,, \tag{31}$$

$$\mathrm{i}G^{<}(\boldsymbol{r}_2-\boldsymbol{r}_1,t) = -\left\langle \hat{c}^{\dagger}_{\boldsymbol{r}_1}(0)\hat{c}_{\boldsymbol{r}_2}(t)\right\rangle_{\beta} = -\frac{1}{Z}\sum_{\boldsymbol{g},m} \mathrm{e}^{-\beta E_m(\boldsymbol{g})}\langle\psi_m(\boldsymbol{g})|\hat{c}^{\dagger}_{\boldsymbol{r}_1}\,\mathrm{e}^{\mathrm{i}\hat{H}_{\mathrm{eff}}t}\hat{c}_{\boldsymbol{r}_2}\mathrm{e}^{-\mathrm{i}\hat{H}_{\mathrm{eff}}t}|\psi_m(\boldsymbol{g})\rangle\,. \tag{32}$$

Transforming into the orthogonal fermion picture, we have

$$\begin{aligned}\mathrm{i}G^{>}(\boldsymbol{r}_2-\boldsymbol{r}_1,t) &= +\sum_{\boldsymbol{g},m}\frac{\mathrm{e}^{-\beta E_m(\boldsymbol{g})}}{Z}\langle\boldsymbol{g}|\otimes\langle\varphi_m(\boldsymbol{g})|\,\mathrm{e}^{\mathrm{i}\hat{H}'t}\sigma^z_{\boldsymbol{r}_2}\hat{c}_{\boldsymbol{r}_2}\mathrm{e}^{-\mathrm{i}\hat{H}'t}\sigma^z_{\boldsymbol{r}_1}\hat{c}^{\dagger}_{\boldsymbol{r}_1}|\varphi_m(\boldsymbol{g})\rangle\otimes|\boldsymbol{g}\rangle \\ &= +\sum_{\boldsymbol{g},m}\frac{\mathrm{e}^{-\beta E_m(\boldsymbol{g})}}{Z}\langle\boldsymbol{g}'_{\boldsymbol{r}_2}|\boldsymbol{g}'_{\boldsymbol{r}_1}\rangle\langle\varphi_m(\boldsymbol{g})|\,\mathrm{e}^{\mathrm{i}\hat{H}_{\mathrm{sub}}(\boldsymbol{g})t}\hat{c}_{\boldsymbol{r}_2}\mathrm{e}^{-\mathrm{i}\hat{H}_{\mathrm{sub}}\left(\boldsymbol{g}'_{\boldsymbol{r}_1}\right)t}\hat{c}^{\dagger}_{\boldsymbol{r}_1}|\varphi_m(\boldsymbol{g})\rangle\,, \end{aligned}\tag{33}$$

$$\begin{aligned}\mathrm{i}G^{<}(\boldsymbol{r}_2-\boldsymbol{r}_1,t) &= -\sum_{\boldsymbol{g},m}\frac{\mathrm{e}^{-\beta E_m(\boldsymbol{g})}}{Z}\langle\boldsymbol{g}|\otimes\langle\varphi_m(\boldsymbol{g})|\,\sigma^z_{\boldsymbol{r}_1}\hat{c}^{\dagger}_{\boldsymbol{r}_1}\mathrm{e}^{\mathrm{i}\hat{H}'t}\sigma^z_{\boldsymbol{r}_2}\hat{c}_{\boldsymbol{r}_2}\mathrm{e}^{-\mathrm{i}\hat{H}'t}|\varphi_m(\boldsymbol{g})\rangle\otimes|\boldsymbol{g}\rangle \\ &= -\sum_{\boldsymbol{g},m}\frac{\mathrm{e}^{-\beta E_m(\boldsymbol{g})}}{Z}\langle\boldsymbol{g}'_{\boldsymbol{r}_2}|\boldsymbol{g}'_{\boldsymbol{r}_1}\rangle\langle\varphi_m(\boldsymbol{g})|\hat{c}^{\dagger}_{\boldsymbol{r}_1}\,\mathrm{e}^{\mathrm{i}\hat{H}_{\mathrm{sub}}\left(\boldsymbol{g}'_{\boldsymbol{r}_1}\right)t}\hat{c}_{\boldsymbol{r}_2}\mathrm{e}^{-\mathrm{i}\hat{H}_{\mathrm{sub}}(\boldsymbol{g})t}|\varphi_m(\boldsymbol{g})\rangle\,. \end{aligned}\tag{34}$$

Here $|\boldsymbol{g}'_{\boldsymbol{r}}\rangle = \sigma^z_{\boldsymbol{r}}|\boldsymbol{g}\rangle$. This means that the background charge distribution $\boldsymbol{g}'_{\boldsymbol{r}}$ is opposite from $\boldsymbol{g}$ at the site $\boldsymbol{r}$. Therefore we have $\langle\boldsymbol{g}'_{\boldsymbol{r}_2}|\boldsymbol{g}'_{\boldsymbol{r}_1}\rangle = \delta_{\boldsymbol{r}_2,\boldsymbol{r}_1}$. This indicates that single particle(hole) excitation cannot propagate, since they are bound with local spins (19). Then we obtain

$$\mathrm{i}G^{>}(\boldsymbol{r}_2-\boldsymbol{r}_1,t) = +\delta_{\boldsymbol{r}_2,\boldsymbol{r}_1}\sum_{\boldsymbol{g}} p_{\boldsymbol{g}}S^{>}_{\boldsymbol{g}}(\boldsymbol{r},t)\,, \tag{35}$$

$$\mathrm{i}G^{<}(\boldsymbol{r}_2-\boldsymbol{r}_1,t) = -\delta_{\boldsymbol{r}_2,\boldsymbol{r}_1}\sum_{\boldsymbol{g}} p_{\boldsymbol{g}}S^{<}_{\boldsymbol{g}}(\boldsymbol{r},t)\,, \tag{36}$$

where

$$S^{>}_{\boldsymbol{g}}(\boldsymbol{r},t) = \frac{\mathrm{Tr}\left\{\mathrm{e}^{-\beta\hat{H}_{\mathrm{sub}}(\boldsymbol{g})}\,\mathrm{e}^{\mathrm{i}\hat{H}_{\mathrm{sub}}(\boldsymbol{g})t}\hat{c}_{\boldsymbol{r}}\,\mathrm{e}^{-\mathrm{i}\hat{H}_{\mathrm{sub}}\left(\boldsymbol{g}'_{\boldsymbol{r}}\right)t}\hat{c}^{\dagger}_{\boldsymbol{r}}\right\}}{\mathrm{Tr}\left\{\mathrm{e}^{-\beta\hat{H}_{\mathrm{sub}}(\boldsymbol{g})}\right\}}, \tag{37}$$

$$S^{<}_{\boldsymbol{g}}(\boldsymbol{r},t) = \frac{\mathrm{Tr}\left\{\mathrm{e}^{-\beta\hat{H}_{\mathrm{sub}}(\boldsymbol{g})}\hat{c}^{\dagger}_{\boldsymbol{r}}\,\mathrm{e}^{\mathrm{i}\hat{H}_{\mathrm{sub}}\left(\boldsymbol{g}'_{\boldsymbol{r}}\right)t}\hat{c}_{\boldsymbol{r}}\,\mathrm{e}^{-\mathrm{i}\hat{H}_{\mathrm{sub}}(\boldsymbol{g})t}\right\}}{\mathrm{Tr}\left\{\mathrm{e}^{-\beta\hat{H}_{\mathrm{sub}}(\boldsymbol{g})}\right\}}, \tag{38}$$

and $p_{\boldsymbol{g}} = \mathrm{Tr}\{\mathrm{e}^{-\beta\hat{H}_{\mathrm{sub}}(\boldsymbol{g})}\}/\sum_{\boldsymbol{g}}\mathrm{Tr}\{\mathrm{e}^{-\beta\hat{H}_{\mathrm{sub}}(\boldsymbol{g})}\}$. Consequently the momentum-resolved radio-frequency spectrum shows no dispersion at any given temperature, $A_{\mathrm{ab/em}}(\boldsymbol{k},\omega) = A_{\mathrm{ab/em}}(\omega)$. In addition, adding (removing) the $\hat{c}$-fermions to (from) the system, will flip the local spins, which will create a local impurity potential for the orthogonal fermions. This process is similar to x-ray absorption or emission in solid materials.[35–40] The non-dispersion relationship can be understood in this way: the local gauge symmetries separate the Hilbert space into different subspaces, and these subspaces are mutually orthodox and labeled with different $\boldsymbol{g}$. As argued in Ref. [34], adding ($\hat{c}^{\dagger}_{\boldsymbol{r}_1}$) or removing ($\hat{c}_{\boldsymbol{r}_1}$) a fermion will scatter the state $|\psi_m(\boldsymbol{g})\rangle$ in the subsector labeled with $\boldsymbol{g}$ into the subsector labeled with $\boldsymbol{g}'_{\boldsymbol{r}_1}$. And $\boldsymbol{g}'_{\boldsymbol{r}_1}$, as denoted as earlier, is opposite to $\boldsymbol{g}$ at site $\boldsymbol{r}_1$. To return to the subsector labeled by $\boldsymbol{g}$, one has to remove or add a fermion at the same site otherwise the system will be excited to other subsectors. Such a constraint gives a δ-function in Eqs. (35) and (36). After Fourier transformation, that leads to a spectrum without dispersion.

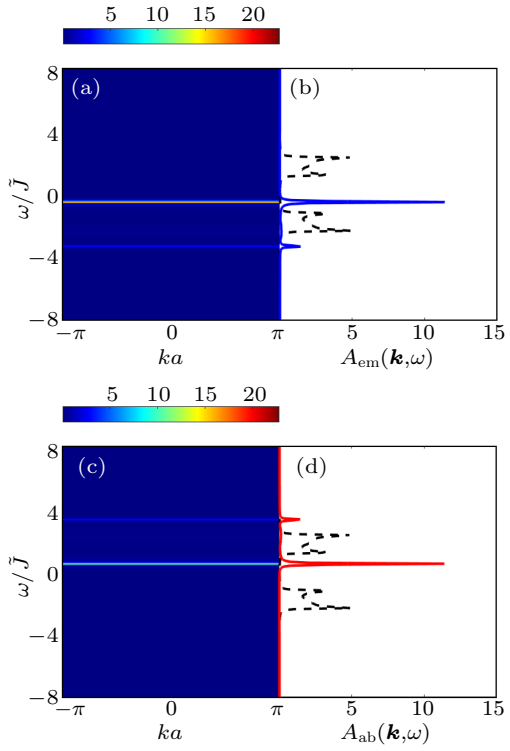


Fig. 3. (a), (c) Momentum resolved radio-frequency emission or absorption spectrum function for a half-filled one-dimensional lattice at zero temperature. (b), (d) Radio-frequency emission or absorption spectrum function at a given momentum. The dashed line is the single-particle density of state in a spin density wave background charge distribution. The calculation is done in a lattice with length 100 and $\tilde{\Omega}/\tilde{J} = 0.6$.

Since $\hat{H}_{\mathrm{sub}}(\boldsymbol{g})$ is quadratic, we can calculate $S^{>}_{\boldsymbol{g}}(\boldsymbol{r},t)$, $S^{<}_{\boldsymbol{g}}(\boldsymbol{r},t)$ and $p_{\boldsymbol{g}}$ via the trace formula.[40] We obtain

$$\begin{aligned}S^{>}_{\boldsymbol{g}}(\boldsymbol{r},t) &= \det\left[1-f_{\boldsymbol{g}}+U(t)f_{\boldsymbol{g}}\right] \\ &\quad\times\langle\boldsymbol{r}|\left[U^{-1}(t)+\frac{f_{\boldsymbol{g}}}{1-f_{\boldsymbol{g}}}\right]^{-1}\mathrm{e}^{-\mathrm{i}H_{\mathrm{sub}}(\boldsymbol{g})t}|\boldsymbol{r}\rangle\,, \end{aligned}\tag{39}$$

$$\begin{aligned}S^{<}_{\boldsymbol{g}}(\boldsymbol{r},t) &= \det\left[1-f_{\boldsymbol{g}}+f_{\boldsymbol{g}}U^{-1}(t)\right] \\ &\quad\times\langle\boldsymbol{r}|\left[U^{-1}(t)+\frac{1-f_{\boldsymbol{g}}}{f_{\boldsymbol{g}}}\right]^{-1}\mathrm{e}^{-\mathrm{i}H_{\mathrm{sub}}(\boldsymbol{g})t}|\boldsymbol{r}\rangle\,, \end{aligned}\tag{40}$$

$$p_{\boldsymbol{g}} = \frac{\det\left(f_{\boldsymbol{g}}^{-1}\right)}{\sum_{\boldsymbol{g}} \det\left(f_{\boldsymbol{g}}^{-1}\right)}, \tag{41}$$

where

$$U(t) = \mathrm{e}^{-\mathrm{i}H_{\mathrm{sub}}\left(\boldsymbol{g}'_{\boldsymbol{r}}\right)t}\,\mathrm{e}^{\mathrm{i}H_{\mathrm{sub}}(\boldsymbol{g})t}, \quad f_{\boldsymbol{g}} = [\mathrm{e}^{-\beta H_{\mathrm{sub}}(\boldsymbol{g})}+1]^{-1}.$$

The zero temperature spectrum is plotted in Fig. 3. The dashed line is the single-particle density of state in a spin density wave background charge distribution. As we discussed above, the spectra are dispersionless and exhibit in-gap peaks, which imply bound states of the $\hat{c}$-fermions and local spins. The finite temperature spectra are plotted in Fig. 4. Note that when temperature increases, the peaks in spectra are broadened, indicating melting of the SDW of background local spins.

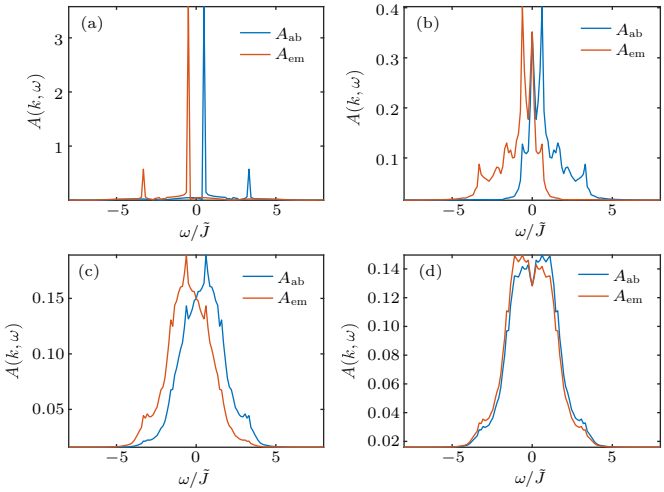


Fig. 4. Absorption and emission spectra at different finite temperatures. The blue lines are absorption spectra and the red lines are emission spectra: (a) $k_{\mathrm{B}}T/\tilde{J}=0.02$, (b) $k_{\mathrm{B}}T/\tilde{J}=0.5$, (c) $k_{\mathrm{B}}T/\tilde{J}=2$, (d) $k_{\mathrm{B}}T/\tilde{J}=10$. The simulation is on a one-dimensional lattice with length 10, and $\tilde{\Omega}/\tilde{J}=0.6$ at half fillings.

5. Dynamical localization

After investigating the absence of a dispersion relationship in the effective Hamiltonian, we now turn our attention to another property, that is, dynamical localization. Consider the time evolution of the initial states

$$|\psi(0)\rangle = \hat{U}^{\dagger}|\varphi(0)\rangle \otimes \prod_{\boldsymbol{r}} |\uparrow\rangle_{\boldsymbol{r}}, \tag{42}$$

where $|\varphi(0)\rangle$ is the initial state of orthogonal fermions and $|\uparrow\rangle_{\boldsymbol{r}}$ is the local eigenstate of $\sigma^z_{\boldsymbol{r}}$, $\sigma^z_{\boldsymbol{r}}|\uparrow\rangle_{\boldsymbol{r}} = |\uparrow\rangle_{\boldsymbol{r}}$. One can expand $|\uparrow\rangle_{\boldsymbol{r}}$ by the local eigenstates of $\hat{G}'_{\boldsymbol{r}}$ as $|\uparrow\rangle_{\boldsymbol{r}} = \frac{1}{2}(|+1\rangle_{\boldsymbol{r}} + |-1\rangle_{\boldsymbol{r}})$. So the initial state can be recast as

$$|\psi(0)\rangle = \sqrt{2}^{-N_{\mathrm{s}}}\hat{U}^{\dagger}|\varphi(0)\rangle \otimes \sum_{\boldsymbol{g}} |\boldsymbol{g}\rangle, \tag{43}$$

where N_{s} is the number of lattice site. Note that this wave function is a superposition of different subspaces. If we focus on the behavior of the fermions, the expectation value of a fermion operator reads

$$\langle O(t)\rangle = \frac{1}{2^{N_{\mathrm{s}}}}\sum_{\boldsymbol{g}} \langle\varphi(0)|\,\mathrm{e}^{\mathrm{i}\hat{H}_{\mathrm{sub}}(\boldsymbol{g})t} O \mathrm{e}^{-\mathrm{i}\hat{H}_{\mathrm{sub}}(\boldsymbol{g})t}\,|\varphi(0)\rangle. \tag{44}$$

We can see that $\mathrm{e}^{-\mathrm{i}\hat{H}_{\mathrm{sub}}(\boldsymbol{g})t}|\varphi(0)\rangle$ is the time evolution of the non-interacting orthogonal fermions in a subsector with given background charge distribution. The summation is identical to the ensemble average of the orthogonal fermions moving in disorder potential. So this dynamics is similar to the Anderson model, expect that the potential here has a binary distribution rather than a uniform distribution. In one or two dimensions, this dynamics exhibits localization.[41–46] However, if we choose the initial state $\hat{U}^{\dagger}|\varphi(0)\rangle \otimes \prod_{\boldsymbol{r}}|+1\rangle_{\boldsymbol{r}}$, which is in one subsector, the orthogonal fermions feel a uniform potential with no background charge fluctuations. Consequently, localization phenomena are absent in this scenario.

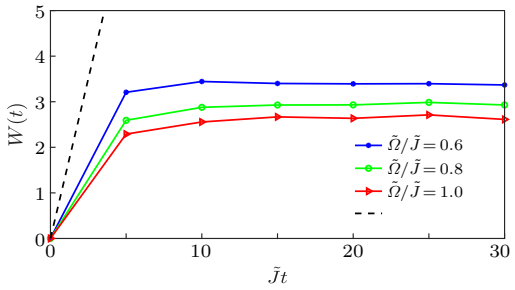


Fig. 5. Wavepacket spreading of one fermion in a one-dimensional lattice gauge field. The initial state of the solid lines is $\hat{U}^{\dagger}\hat{c}^{\dagger}_{\mathbf{0}}|0\rangle \otimes \prod_{\boldsymbol{r}}|\uparrow\rangle_{\boldsymbol{r}}$, while the initial state of the dashed line is $U^{\dagger}\hat{c}^{\dagger}_{\mathbf{0}}|0\rangle \otimes \prod_{\boldsymbol{r}}|+1\rangle_{\boldsymbol{r}}$. The simulation is done on a lattice with length 21.

Moreover, we calculate the spreading of a single fermion wavepacket in one dimension (see Fig. 5). Starting from the uniform background charges, the width of the wavepacket, $W = \sqrt{\langle\sum_{\boldsymbol{r}} \boldsymbol{r}^2\hat{c}^{\dagger}_{\boldsymbol{r}}\hat{c}_{\boldsymbol{r}}\rangle - \langle\sum_{\boldsymbol{r}}\boldsymbol{r}\hat{c}^{\dagger}_{\boldsymbol{r}}\hat{c}_{\boldsymbol{r}}\rangle^2}$, grows linearly with time. However, if the initial state is a superposition state the width is saturated at long times, so the disorder effect in the dynamics is led by the background charge fluctuation, which is the consequence of the superposition initial states. It should be emphasized that local gauge symmetry is crucial in these dynamic localizations. Since local gauge symmetry separates the Hilbert space into different subspaces, different subspaces have different configurations of background gauge charges. When we start from a superposition of different subspaces, the fluctuations of the background gauge charges play the role of local disorder potential of fermions. That makes the fermions localized.

6. Summary and outlooks

We propose a Floquet approach to simulate a simple lattice gauge model. Our method is feasible with current experimental techniques, and is adaptable to systems in one, two or three dimensions. The effective Hamiltonian is obtained

by keeping to the zeroth order of $1/\omega$ expansion. The next order processes break the local gauge symmetry. However, those terms are highly suppressed in the large driving frequency limit, such that the gauge-invariant dynamics will not be affected in the typical time scale of the experiment. The predicted dispersionless spectrum can be observed via widely used radio-frequency spectroscopy in ultracold atomic systems. Dynamic localization can be detected by *in situ* measurement in optical lattices.

Acknowledgements

Project supported by the National Natural Science Foundation of China (Grant Nos. GG2030007011 (WZ), GG203004045 (WZ), and 12374477(PZ)) and Innovation Program for Quantum Science and Technology (Grant No. 2021ZD0302004 (WZ)).

References

[1] Kogut J B 1979 *Rev. Mod. Phys* **51** 659
[2] Balents L 2010 *Nature* **464** 199
[3] Read N and Sachdev S 1991 *Phys. Rev. Lett.* **66** 1773
[4] Jalabert R A and Sachdev S 1991 *Phys. Rev. B* **44** 686
[5] Baskaran G and Anderson P W 1988 *Phys. Rev. B* **37** 580
[6] Read N and Sachdev S 1990 *Phys. Rev. B* **42** 4568
[7] Affleck I and Marston J B 1988 *Phys. Rev. B* **37** 3774
[8] Senthil T and Fisher M P A 2020 *Phys. Rev. B* **62** 7850
[9] Kivelson S A, Rokhsar D S and Sethna J P 1987 *Phys. Rev. B* **35** 8865
[10] Moessner R, Sondhi S L and Fradkin E 2001 *Phys. Rev. B* **65** 024504
[11] Wiese U 2013 *Ann. Phys. (Berlin)* **525** 777
[12] Assaad F F and Grover T 2016 *Phys. Rev. X* **6** 041049
[13] Martinez E A, Muschik C A, Schindler P, Nigg D, Erhard A, Heyl M, Hauke Pp, Dalmonte M, Monz T, Zoller P and Blatt R 2016 *Nature* **534** 516
[14] Zohar E, Farace E A, Reznik B and Cirac J I 2017 *Phys. Rev. Lett.* **118** 070501
[15] Barbiero L, Schweizer C, Aidelsburger M, Demler E, Goldman N and Fa G 2019 *Sci. Adv.* **5** 7444
[16] Lin Y J, Compton R L, Jiménez-García K, Phillips W D, Porto J V and Spielman I B 2011 *Nat. Phys.* **7** 531
[17] Lin Y J, Compton R L, Jiménez-García K, Porto J V and Spielman I B 2009 *Nature* **462** 628
[18] Lin Y J, Jiménez-García K and Spielman I B 2011 *Nature* **471** 83
[19] Wu Z, Zhang L, Sun W, Xu X T, Wang B Z, Ji S C, Deng Y, Chen S, Liu X J and Pan J W 2016 *Science* **354** 83
[20] Clark L W, Anderson B M, Feng L, Gaj A, Levin K and Chin C 2018 *Phys. Rev. Lett.* **121** 030402
[21] Görg F, Sandholzer K, Minguzzi J, Desbuquois R, Messer M and Esslinger T 2019 *Nat. Phys.* **15** 1161
[22] Kroeze R M, Guo Y and Lev B L 2019 *Phys. Rev. Lett.* **123** 160404
[23] Schweizer C, Grusdt F, Berngruber M, Barbiero L, Demler E, Goldman N, Bloch I and Aidelsburger M 2019 *Nat. Phys.* **15** 1168
[24] Yang B, Sun H, Ott R, Wang H Y, Zache T V, Halimeh J C, Yuan Z S, Hauke P and Pan J W 2020 *Nature* **587** 392
[25] Mil A, Zache T V, Hegde A, Xia A, Bhatt R P, Oberthaler M K, Hauke P, Berges J and Jendrzejewski F 2020 *Science* **367** 1128
[26] Zhou Z Y, Su G X, Halimeh J C, Ott R, Sun H, Hauke P, Yang B, Yuan Z S, Berges J and Pan J W 2022 *Science* **377** 311
[27] Wang H Y, Zhang W Y, Yao Z Y, Liu Y, Zhu Z H, Zheng Y G, Wang X K, Zhai H, Yuan Z S and Pan J W 2023 *Phys. Rev. Lett.* **131** 050401
[28] Zhang W Y, Liu Y, Cheng Y, He M G, Wang H Y, Wang T Y, Zhu Z H, Su G X, Zhou Z Y, Zheng Y G, Sun H, Yang B, Hauke P, Zheng W, Halimeh J C, Yuan Z S and Pan J W arXiv:2306.11794
[29] Rüegg A, Huber S D and Sigrist M 2010 *Phys. Rev. B* **81** 155118
[30] Nandkishore R, Metlitski M A and Senthil T 2012 *Phys. Rev. B* **86** 045128
[31] Gazit S, Assaad F F and Sachdev S 2020 *Phys. Rev. X* **10** 041057
[32] Chen C, Xu X Y, Qi Y and Meng Z Y 2020 *Chin. Phys. Lett.* **37** 047103
[33] Prosko C, Lee S P and Maciejko J 2017 *Phys. Rev. B* **96** 205104
[34] Qi H Y and Zheng W 2024 *Phys. Rev. Res.* **6** 013047
[35] Anderson P W 1967 *Phys. Rev.* **164** 352
[36] Mahan G D 1967 *Phys. Rev.* **153** 882
[37] Roulet B, Gavoret J and Nozières P 1969 *Phys. Rev.* **178** 1072
[38] Nozières P, Roulet B and Gavoret J 1969 *Phys. Rev.* **178** 1084
[39] Nozières P and De Dominicis C T 1969 *Phys. Rev.* **178** 1097
[40] Benjamin D, Abanin D, Abbamonte P and Demler E 2013 *Phys. Rev. Lett.* **110** 137002
[41] Smith A, Knolle J, Kovrizhin D L and Moessner R 2017 *Phys. Rev. Lett.* **118** 266601
[42] Brenes M, Dalmonte M, Heyl M and Scardicchio A 2018 *Phys. Rev. Lett.* **120** 030601
[43] Smith A, Knolle J, Moessner R and Kovrizhin D L 2018 *Phys. Rev. B* **97** 245137
[44] Yarloo H, Mohseni-Rajaee M and Langari A 2019 *Phys. Rev. B* **99** 054403
[45] Yao Z, Liu C, Zhang P and Zhai H 2020 *Phys. Rev. B* **102** 104302
[46] Papaefstathiou I, Smith A and Knolle J 2020 *Phys. Rev. B* **102** 165132